Magnetic Field Spatial Fourier Analysis: A New Opportunity for High Resolution Current Localization

F. Infante[a,*], P. Perdu[b], H.B. Kor[b,c], C.L. Gan[c], D. Lewis[d]

[a] *Intraspec Technologies, 29 rue Jeanne Marvig, 31400 Toulouse, France*
[b] *CNES, 18 Avenue E. Belin, 31401 Toulouse, France*
[c] *Nanyang Technological University, School of Materials Science & Engineering, 50 Nanyang Avenue, Singapore 639798.*
[d] *Université Bordeaux 1, 351 Cours de la Libération, 33405 Talence, France*

Abstract

Magnetic microscopy has proven its usefulness throughout the years. It allows current localization with a certain degree of precision by using an inversion algorithm to invert the Biot-Savart law. The goal is to obtain the current distribution once the magnetic field is given. However, in order to obtain a stable solution, the magnetic data is severely low-pass filtered in the spatial Fourier domain, and some important information is lost. In this paper, the contribution given by the different spatial frequencies was studied: it was demonstrated how this information can be used to obtain additional information regarding the position of the currents. A comparative study between the theoretical approach and the application to the measurements is also shown.

1. Introduction

When an electronic component fails, there is a need to perform a failure analysis in order to understand the root cause of the failure. The failure can occur in all the phases of the development of the technology, i.e. from the production of the first prototypes (which very often require a better comprehension before being sent to the final stage of production) to the final product, as well as the failed components coming out from the field: what is usually called the customer returns.

In all the cases, the understanding of the root cause of the failure is of fundamental importance for the constant improvement of the microelectronic technologies. The best way to improve the reliability of devices is to implement corrective measures on the process and design stages which are suggested by the results of a correctly done failure analysis.

One important step in the failure analysis process is the defect localization, which is very often the most difficult to perform. Many different techniques have been developed to solve this problem for a very wide range of cases.

In this paper, an analysis of the Fourier spectra of the acquisitions of the magnetic field was proposed. The objective is to extract additional information for the precise localization of the currents, and therefore to

* Corresponding author. fulvio.infante@intraspectechnologies.com
Tel: +33 (0)5 612 745 54; Fax: +33 (0)5 612 747 32

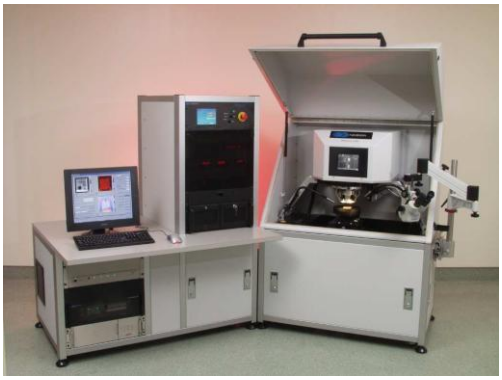

Fig. 1. Magnetic Microscope.

increase the localization accuracy. This can be then used to evaluate the precise distance between two flowing currents.

2. Magnetic microscopy

Among the several techniques which are used to localize the failures in the electronic components, magnetic microscopy allows the analyst to pre-localize the defects in a non-destructive, non-invasive and contactless way [1]. The magnetic field is in fact not shielded by the presence of non-ferromagnetic materials, such as the majority of those used in the microelectronics packages.

2.1. Magnetic Current Imaging

The analyses for this paper were performed starting from the measurements of the magnetic field done by the magnetic microscope, shown in Fig. 1. The technique used by this tool is called Magnetic Current Imaging (MCI), and is based on the inversion of the Biot-Savart law [2]. It is known in fact that, whenever there is a current flowing, a magnetic field is generated. In the case of the quasi-static approximation, the generated magnetic field can be evaluated from the Biot-Savart law, as shown in Eq. 1:

$$\vec{B}(\vec{r}) = \frac{\mu_0}{4\pi} \iiint \frac{\vec{J}(\vec{r}') \times (\vec{r} - \vec{r}')}{|\vec{r} - \vec{r}'|^3} dr'^3 \qquad (1)$$

The MCI technique then uses a spatial Fourier transform approach to invert Eq. 1, in order to obtain the current distribution *J*, once the *z* component of the magnetic field is measured [3]. After applying the Fourier transform to both members of Eq. 1, the x

Fig. 2. MCI results for currents 250 µm from each other.

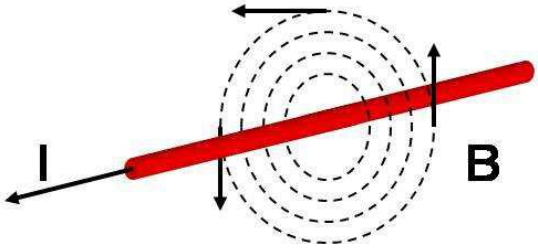

Fig. 3. Magnetic field generated by a current line.

component of the current distribution can be evaluated as follows:

$$j_y(k_x, k_y) = \frac{b_x(k_x, k_y, z)}{g(k_x, k_y, z)} \qquad (2)$$

where k_x and k_y are the component of the spatial frequency vector, and *g* is the Fourier transform of the Green function.

2.2. MCI limitations

The Green function tends towards zero with the increase of the spatial frequencies: therefore, in order to have a meaningful solution, the b_x function needs to be multiplied by a cut-off filter, at a fixed frequency k_W: the spatial transform of the magnetic field has to be severely low-pass filtered [4].

In this way, the information given by the higher spatial frequencies is lost. Even if this approach gives a very elegant solution to the inverse problem, it does not allow the distinction of very close currents. An example is shown in Fig. 2: here two current lines are mapped with the MCI algorithm, when the sensor is at 100 and 1000 µm distance from the currents, respectively. It is not possible to distinguish between the currents scanned at a working distance of 1mm.

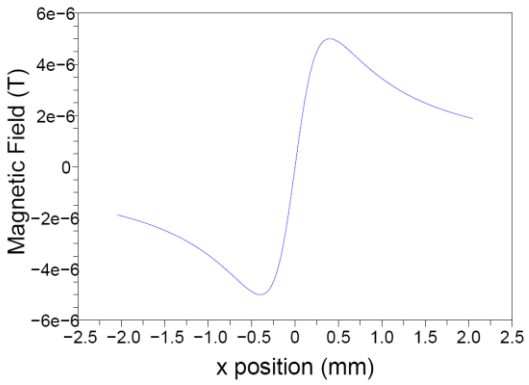

Fig. 4. B_z generated by a current line.

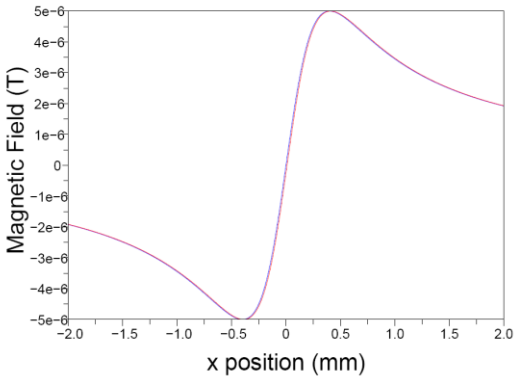

Fig. 5. B_z generated by two current lines 10 μm apart from each other.

2.3. Measurements of the field

As stated previously, the magnetic field generated by a current line is distributed following Eq.1. A schematic representation of this law is shown in Fig. 3. The magnetic microscope only acquires the *z* component of the magnetic field over a *x*-*y* plane, which is enough to generate the current distribution layout.

Eq.1 also shows that if the current *I* is a DC current, the resulting magnetic field will also be DC. However, it is well known that the static magnetic field contains various contributions given by the environment. The best way to increase the Signal-to-Noise Ratio (SNR) is that of using a lock-in approach. The electrical conductor is stimulated with an AC current at a pre-known frequency; the signal is then acquired and filtered through a lock-in amplifier. The resulting signal is then shifted back to the DC frequency.

The frequency chosen for the signal acquisition is 5333 Hz. This frequency was chosen for not being a multiple of the 50 Hz frequency, which is where most of the magnetic noise is situated due to the standard electrical apparatus. The magnetic sensor which is used for the whole analysis reported here is a Superconducting Quantum Interference Device (SQUID). The SQUID has a very high sensitivity, as it can acquire fields as low as a few nT. Its superconducting nature allows also the detection of relatively high frequency fields, up to a few hundred MHz.

The typical shape of the *z* component of the B field is shown in Fig. 4: the position of the current is given by the intersection of the curve on the *x*-axis. However, there are many reasons why the precise location of the current cannot be simply given by this measurement.

First of all, the presence of other currents nearby can create a distortion of the curve. Furthermore, even a small vertical offset of the measurement can considerably displace the zero value on either sides of the positive or the negative regime, and the position evaluated in this way would be wrong. The MCI technique overcomes these limitations, but also introduces some new ones, mostly given by the necessity to filter the magnetic data in order to stabilize the results.

3. Spatial Fourier analysis

3.1. Introduction

In this paper, a different approach to the problem of the current localization, which is based on the analysis of the phase spectrum in the spatial Fourier domain, was proposed. The purpose is to extract the position information of the current lines by studying the phase spectrum first, and then the amplitude spectrum. The analysis was first performed on a theoretical noise-free magnetic curve generated analytically, and then compared to the analysis of a real measured acquisition. With this approach, the distance between two very close parallel current lines lying on the same *x*-*y* plane can be extracted.

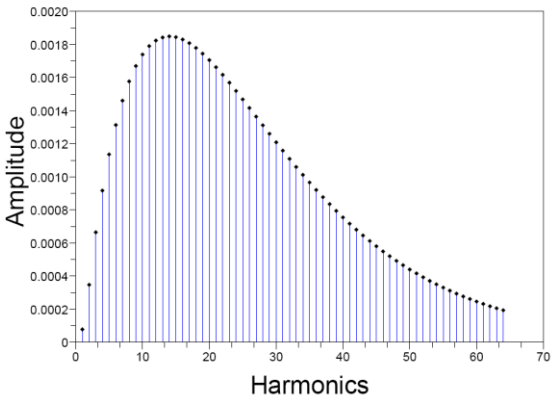

Fig.6. Amplitude spectrum of the difference signal.

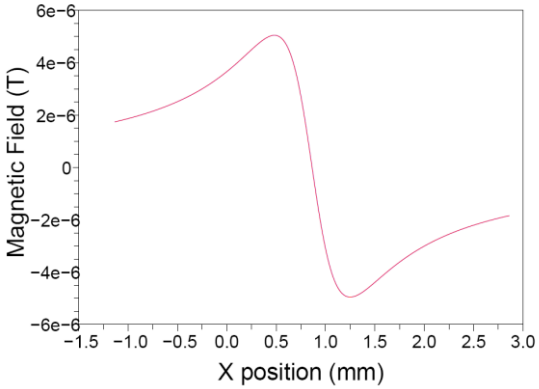

Fig.8. z component measured from the two currents, respectively in red and blue.

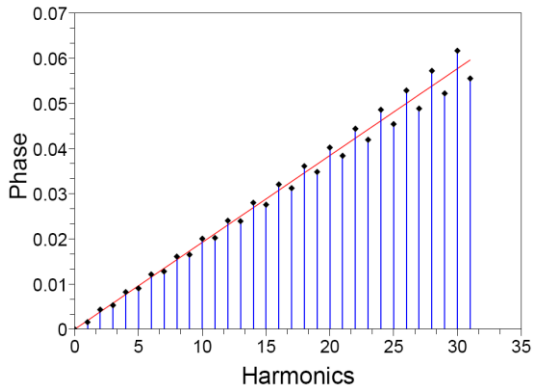

Fig.7. Difference of the phase spectrum signals.

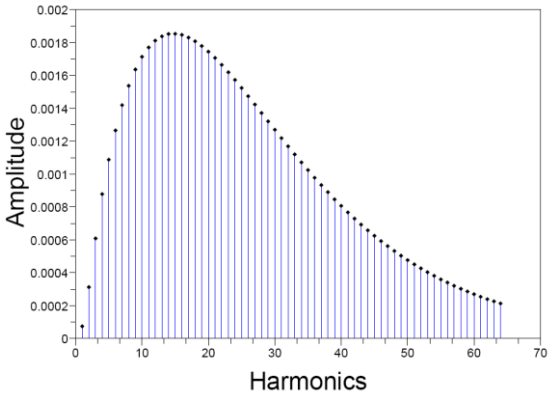

Fig.9. Amplitude spectrum of the difference signal.

3.2. Amplitude and Phase Information

3.2.1. Theoretical study

A first study of the problem was performed on an analytically generated magnetic field. The *z* component of the magnetic field generated by a current flowing along the *y*-axis, acquired on a line on the *x*-axis, at a working distance *z*, at the position x_0 and with a current *I* is given by:

$$B_z(x,z) = \frac{\mu_0 I}{2\pi} \frac{x - x_0}{(x - x_0)^2 + z^2} \tag{3}$$

The geometry simulated is that of two parallel current lines, lying on the same *x*-*y* plane, at a working distance *z* of 400 µm and 10 µm apart from each other, as shown in Fig. 5. The magnetic field curves generated by the two currents are the blue and the red curves, respectively.

The Fourier analysis performed on the difference signal gives interesting results, both on the amplitude and the phase spectra. The spatial pseudo-period chosen for the analysis, S, is 32.768 mm. The value was arbitrary chosen as a power of 2, in order to easily apply the FFT algorithm; however this choice does not preclude any generality to the results obtained. Therefore, the fundamental harmonic is given by:

$$f_1 = \frac{1}{S} = 30.517 m^{-1} \tag{4}$$

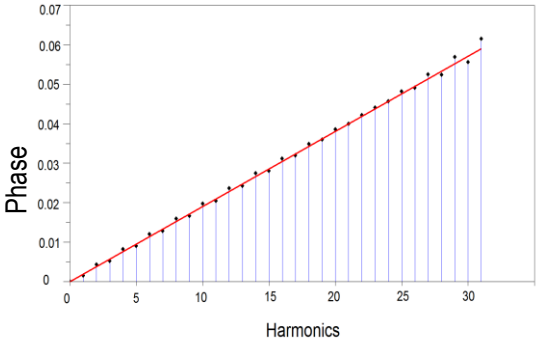

Fig.10. Phase spectrum of the difference signal.

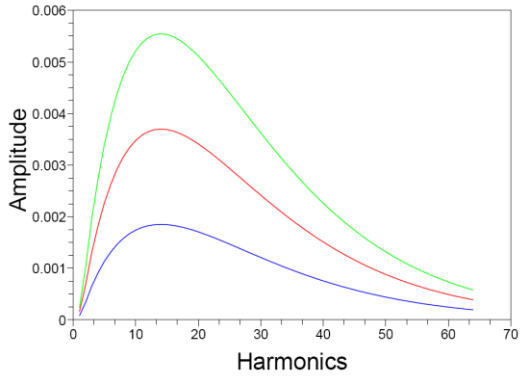

Fig.11. Maximum of the amplitudes of two current lines spaced 1 µm (blue), 2 µm (red) and 3 µm (green) apart (theoretical analysis)

From the amplitude spectrum, which is shown in Fig. 6, it can be seen where the strongest harmonics are situated in frequency. Therefore, to study the phase spectrum, only the first 32 harmonics are considered. It has some sense to stop the study until the 31st harmonic f_{31}, where:

$$f_{31} = 31 \cdot f_1 = 946.044\ m^{-1} \tag{5}$$

The phase spectrum for the first 32 can therefore produce the needed information regarding the shift of the current lines. The phase of the difference signal is in fact given by:

$$\angle B_z = f \cdot \beta \tag{6}$$

where β is the phase shift between the two signals. In Fig. 7, the linear approximation of the function of Eq. 6 is drawn in red, while the dots are the actual phase values. In this case, β = 0.0019175 is obtained. From this value, the shift between the two magnetic curves can be evaluated as follows:

$$Shift = \frac{S \cdot \beta}{2\pi} = 10\mu m \tag{7}$$

3.2.2. Application to the measurements

This technique was then applied to the measurements of the magnetic field generated by two parallel current lines separated by 10 µm. The B_z curves are shown in Fig. 8, in red and blue, respectively. When proceeding to apply the Fast Fourier Transform (FFT) algorithm, the resulting amplitude of the difference signal is shown in Fig. 9. The difference in the phase spectra are shown in Fig. 10. From the phase spectrum, it was possible to evaluate the trend by using the least square method with the constraint of passing through the origin. The resulting β, the angular coefficient of the red straight line of Fig. 10, is 0.0019031, which substituted in the Eq. 7 gives a shift of 9.9 µm, very close to the real 10 µm value.

3.3. More Information from Amplitude

Further FFT experiments were performed on both the theoretically generated magnetic fields and the measurements, by varying the distance between two current lines from 1 µm to 9 µm (in intervals of 1 µm); 10 µm to 200 µm (in intervals of 10 µm) and 300 µm to 1 mm (in intervals of 100 µm). This is to determine if further information can be obtained from the amplitude of the difference signal after FFT.

It was found in the theoretical analysis that for two current lines at different distances apart, the maximum of the amplitude stays at the same harmonic (i.e. harmonic 14) for all the separations of the current lines from 1 µm to 1 mm. A few examples are shown in Fig. 11.

However, when the FFT was performed on the measurements, the maximum of the amplitude was found to be at harmonic 15 at a separation of the two current lines at 1µm apart. The maximums of the amplitudes changed to harmonic 14 at a separation of 150 µm; harmonic 13 at a separation of 500 µm; harmonic 12 at a separation of 700 µm and harmonic 11 at a separation of 900 µm. This is probably due to the presence of noise in the measurements, while the theoretical analysis is noise-free.

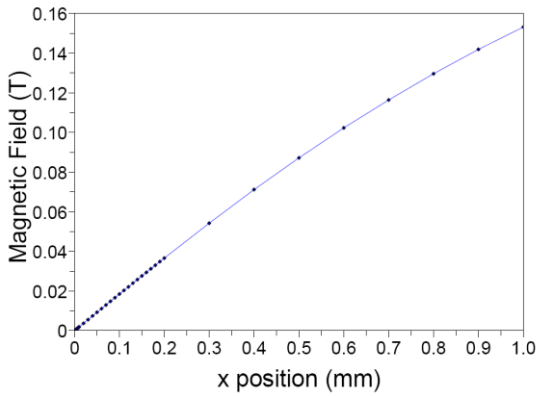

Fig.12. Extraction of current positions from amplitude of the difference signal (theoretical analysis)

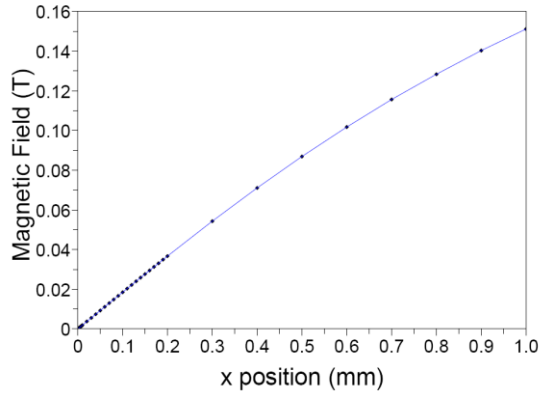

Fig.13. Extraction of current positions from amplitude of the difference signal (measurements)

Nevertheless, the FFT analyses on both the analytically generated and measured magnetic fields provided useful information. Fig. 12 and Fig. 13 show the extraction of the current positions from the amplitude of the difference signal of the theoretical analysis and measurements, respectively.

The theoretical analysis and the measurements again, match very well. From the amplitude information, it is therefore possible to obtain even more precise current positions. This approach will work very well in the linear regime (up to 200 µm) of the graphs in Fig. 14 and Fig. 15. For further separation distances between the two current lines, the approach reaches its limitations. However, for high separation distances, the standard MCI approach is able to give the desired result.

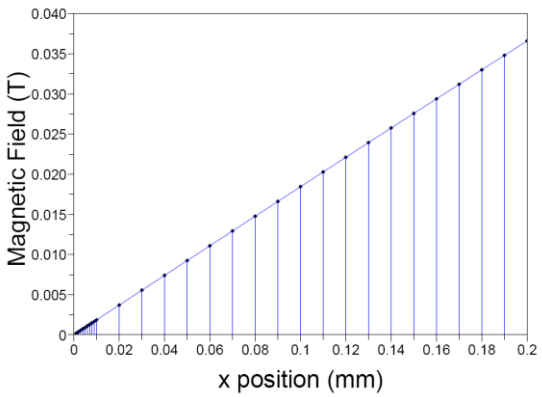

Fig.14. Linear regime (theoretical analysis)

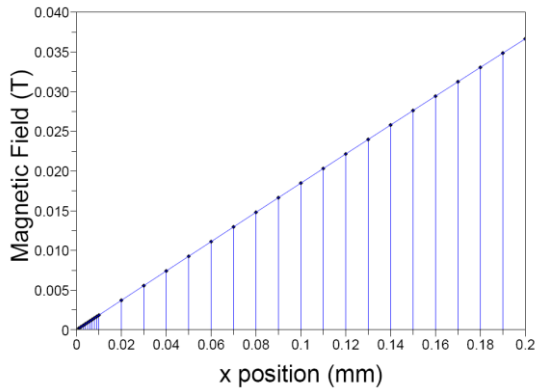

Fig.15. Linear regime (measurements)

3.4. Resolution and localization accuracy

The new approach proposed in this paper shows a big improvement of the localization accuracy of current lines: it is focused on the discrimination of two parallel current lines flowing very closely to each other. In this way, it is possible to obtain a better defect localization, which reduces the need for physical analysis. To some extent, it can be said that this method improves the resolution, even if this remains lower than the theoretical best one. Anyway, putting a value on the resolution strongly depends on the chosen criterion (two different examples are given in [5] and [6]). It has to be noted that the spatial resolution is a quantitative expression, which in some cases can be de-correlated from the actual accuracy for the localization of a current: in most cases, the localization accuracy can be much higher than the spatial resolution.

4. Conclusions

In this paper, it has been demonstrated how it is possible to overcome the present limitations of the MCI technique for localizing current lines which are very close to each other, and when the current-to-sensor distance is significantly bigger than the distance between the currents. The comparison between the theoretical study and the measurements shows an incredible matching: this is mostly due to the good SNR value for the spatial frequencies which have been taken into account.

It has been demonstrated that with this approach, it is possible to obtain useful information about the precise positions of current lines from the phase and amplitude of the difference signal.

For future work, this technique may help to obtain further information about other current parameters, such as the *z* distance.

References

[1] Knauss LA et al. Scanning SQUID Microscopy for Current Imaging. Microelectronics Reliability no. 41, February 2001; pp 1211-1229

[2] Roth BJ, Sepulveda NG, Wikswo Jr JP. Using a magnetometer to image a two-dimensional current distribution. Journal of Applied Physics 65, 1 January 1989; p. 361-372.

[3] Wikswo Jr JP. The magnetic inverse problem for NDE. In Weinstock H, editor. SQUID Sensors: Fundamentals, Fabrication and Applications, Kluwer Academic Publishers; 1996, p.629-695.

[4] Infante F, Perdu P, Lewis D. Magnetic microscopy for 3D devices: Defect localization with high resolution and long working distance on complex system in package. Proceedings of 20th ESREF, 2009; p. 1169-1174.

[5] J. R. Kirtley et al. High-resolution scanning SQUID microscope, Applied Physics Letters 66 (9), 27 February 1995; p. 1138-1140.

[6] C. Dolabdjian et al. Spatial resolution of SQUID magnetometers and comparison with low noise room temperature magnetic sensors. Physica C 368 (2002); p. 80–84.